Catheter Interventions in Congenital Heart Disease—Part I

Guest Editor, Horst Sievert

Applications of Magnetic Resonance Imaging for Cardiac Stem Cell Therapy

CARSTEN RICKERS, M.D.,[1,6] ROBERT GALLEGOS, M.D.,[2] RAVI TEJA SEETHAMRAJU, PH.D.,[1] XIAOEN WANG, M.D.,[1] CORY SWINGEN, M.S.,[1] AVINASH JAYASWAL,[5] ERIC P. RAHRMANN,[5] ZACHARY J. KASTENBERG,[5] CHRISTINA E. CLARKSON, D.V.M., PH.D.,[5] RICHARD BIANCO, B.S.,[4] TIM O'BRIAN, D.V.M., PH.D.,[3] CATHERINE VERFAILLIE, M.D.,[5] R. MORTON BOLMAN III, M.D.,[2] NORBERT WILKE, M.D.,[7] and MICHAEL JEROSCH-HEROLD, PH.D.[1]

From the [1]Cardiovascular MRI Section, Department of Radiology; [2]Department of Cardiovascular and Thoracic Surgery; [3]Division of Veterinary Pathobiology; [4]Experimental Surgical Services; [5]The Stem Cell Institute in the Department of Medicine, University of Minnesota, Minneapolis, Minnesota, U.S.A.; [6]Department of Pediatric Cardiology, University Hospital Hamburg-Eppendorf, Hamburg, Germany; [7]Cardiovascular Center, University of Florida Health Science Center, Jacksonville, Florida, U.S.A.

Background: *The latest generation of interactive cardiac magnetic resonance (MR) scanners has made cardiac interventions with real-time MRI possible. To date, cardiac MRI has been mostly applied to measure myocardial perfusion, viability, and regional function, but now the application of cardiac MRI can be extended to cardiovascular interventions. The purpose of this article is to illustrate the potential of MRI in stem cell therapy for cardiac restoration.*

Methods: *We have applied MRI to (1) interactively target myocardial injections with a novel stem cell delivery catheter, and to compare gadolinium/blue dye injections to pathology; (2) assess myocardial perfusion with MR first pass imaging in an infarct model treated with stem cell therapy versus control animals; (3) measure regional functional changes using myocardial tissue tagging in the same animals.*

Results: *We were able to demonstrate the feasibility and safety of myocardial injections under MR fluoroscopy. The intramyocardial distribution of the blue dye at necropsy correlated well with the extent of gadolinium, as detected with a three-dimensional inversion recovery MR pulse sequence for late enhancement immediately after contrast injection. Preliminary results show that myocardial perfusion reserve and regional wall motion improved in the stem-cell-treated group, compared to a control group.*

Conclusions: *These preliminary results suggest that (1) injections into the LV myocardium can be performed under real-time MRI guidance using a directed catheter approach, and (2) regional myocardial perfusion and function, measured with MRI, both improve after stem cell therapy. This ongoing study demonstrates the potential of MRI for image-guided interventions, combined with detailed evaluation of anatomy, function, perfusion, and viability.*
(J Interven Cardiol 2004;17:37–46)

Introduction

Stem cell therapy has been used as a stimulant for cardiomyoplasty in acute ischemic models.[1,2] Recent developments and improvements of cardiac MR scanners, and ultrafast MRI sequences, have rendered it feasible to acquire images within 80–200 ms, providing fluoroscopic image rates from 5 to15 images/s.[3–19] Thus, MRI can be used for guiding interventional cardiovascular procedures with close to real-time image feedback. MR-guided catheter interventions benefit from several advantages over conventional echocardiographic and X-ray-based techniques for monitoring

Address for reprints: Ravi Teja Seethamraju, Ph.D., Siemens Medical Solutions, USA, Inc, MGH-NMR Center, Building 149, 13th Street, Mail Code 149(2301), Charlestown, Massachusetts 02129-2060. Fax: +1 617 726 7422; e-mail: seethamraju@siemens.com

cardiac stem cell therapy. As a tomographic imaging modality MRI allows the investigator to image arbitrarily oriented cross sections, and to interactively steer the image plane to target designated myocardial areas for stem cell injections. Myocardial targeting is facilitated by the excellent soft tissue contrast achievable by MRI, which is applied for high-resolution anatomical, viability, and perfusion imaging, in the same setting as real-time fluoroscopic imaging.

The purpose of this article is to illustrate initial experiences with MRI for monitoring stem cell therapy applied for cardiac restoration. Specifically, we applied MRI to test a novel stem cell delivery catheter and to demonstrate by injections of gadolinium contrast agent, and blue dye, how one can target by real-time MRI guidance select myocardial regions for injections of therapeutic agents. MR images of the injections were compared to pathology. The delivery method was similar to other methods applied previously for catheter tracking in MRI.[20,21] Secondly, we determined myocardial blood flow with MR perfusion imaging in a large domestic animal infarct model treated with stem cells, by comparison to sham-treated animals. Finally, we also show how regional function measured with MRI with myocardial tissue tagging demonstrates an improvement in regional function as a result of stem cell therapy.

Methods

This study consisted of two arms, namely (1) the investigation of MRI-guided myocardial injections, and (2) longitudinal studies of stem cell therapy. The animals were treated according to the "Principles of Laboratory Animal Care" of the National Society for Medical Research and the "Guide for the Care and Use of Laboratory Animals" (NIH publications, revised 1996). IRB approval was obtained for the study. The experimental procedures were performed under sterile conditions with continuous ECG and oxygen saturation monitoring. General anesthesia was maintained in the intubated animals with 1–2% isoflourane and 3–4 L/min of oxygen at 15 cc/kg of tidal volume.

Animal Model for MRI-guided Myocardial Injections. For the investigation of MRI-guided myocardial injections, we used four healthy adult animals, two dogs, and two pigs (18–36 kg). Vascular access was established via a cut or percutaneous arterial puncture followed by vascular sheath placement into the femoral artery. The animal was then transported to the MRI unit.

Myocardial Ischemia Model. Stem cells have been demonstrated to be present within various organ tissues in the adult.[21,22] Differentiation of adult stem cells into myocyte occurs due to induct with in vitro exposure to specific signal molecules.[23,24] Recently, the ability to induce in vivo transformation of bone marrow derived mesenchymal stem cells into myocytes in the rat has been reported.[25,26]

For the longitudinal MRI studies of stem cell therapy, we used 13 healthy adult male mongrel dogs (24–32 kg). Ten animals survived after surgery and were randomized into two groups of five treated animals and five untreated animals. Myocardial infarcts in the anterior wall were induced by ligating the distal to the first diagonal branch of the left anterior descending coronary artery. For this procedure, the heart was exposed by means of a left thoracotomy through the fourth and fifth intercostals space.

The infarct was allowed to mature for 4 weeks, and during this time cell culture was used to isolate stem cells by a process that has been described previously.[27,28] Four weeks after myocardial infarction, the animals were returned to the operating room for a second thoracotomy. A series of direct myocardial injections of autologous-labeled stem cells ($\sim 1 \times 10^6$ cells/injection) were performed in radial fashion, beginning centrally in the area of ischemia. Similarly, the control animals were injected with an equal amount of stem-cell-free media.

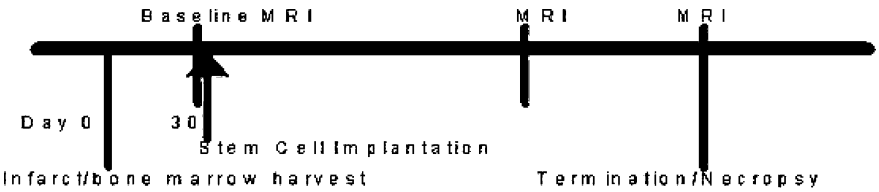

Figure 1. Experimental time line for large animal infarct model with stem cell treatment.

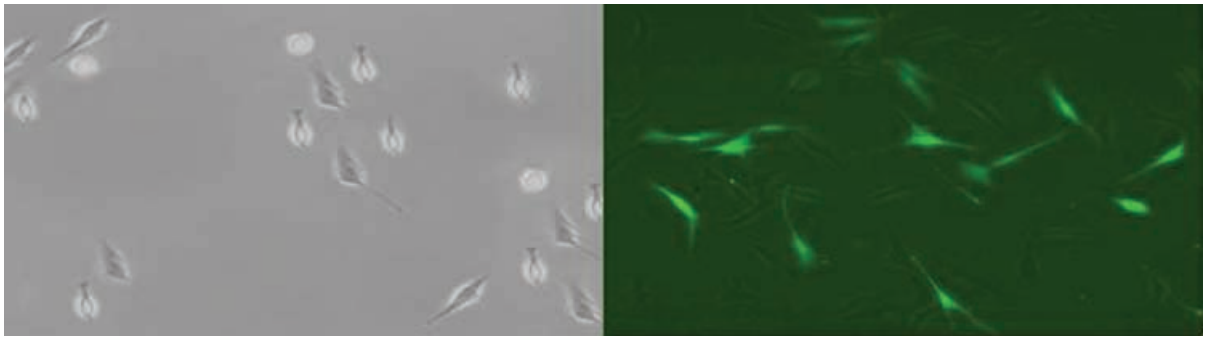

Figure 2. Stem cells before (left) and after (right) reporter gene incorporation (GFP-labeled MAPCs).

Cardiac function, perfusion, and viability were serially monitored by MRI at predetermined time points, both pre- and posttreatment (Fig. 1). The animals were sacrificed at the completion of the study to allow for pathological evaluation and confirmation of stem cell engraftment (Fig. 2).

Catheter Tracking and MRI-guided Myocardial Injections. MR-guided tracking of the delivery catheter and targeting of the infarct were performed on a dedicated cardiac MRI scanner (Sonata, SIEMENS) with a short-bore magnet, operating at field strength of 1.5 Tesla. First, a series of scout images was acquired under interactive user control of the image slice orientation. For positioning of the delivery catheter dedicated guidewires with MRI antenna (Surgi-Vision, N. Chelmsford, MA) were used for high-resolution intravascular imaging. Due to the high signal intensity in the immediate vicinity of the antenna guidewires (Fig. 3),[29–33] a relatively thick slice could be used for catheter tracking by real-time imaging. Real-time MRI was performed with a steady-state free precession pulse sequence ("true FISP"; TR = 1.4 ms, TE = 1.15 ms, flip angle = 40°, 50–60 phase encodings, 128 by 128 image matrix, 7–15 frames/s, 1,400 Hz/pixel, 35 mm slice thickness) (Fig. 4). With the real-time pulse sequence running under interactive user control, a customized delivery catheter (AGA Medical, Golden Valley) was advanced over the antenna guidewire toward the LV and different myocardial regions could be targeted. The antenna guidewire was then replaced with the stem cell injection catheter (Boston Scientific, Plymouth, Minnesota) (Fig. 5). A stable catheter position was confirmed by MRI and myocardial injections of gadolinium mixed with blue dye were monitored by high-resolution real-time imaging (Fig. 6) (sequence

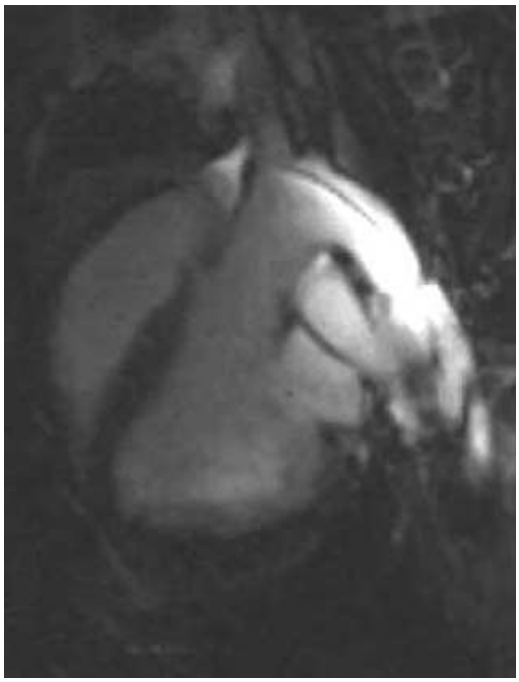

Figure 3. Snapshots of guidewire tracking under real-time MRI in the aortic arch using a loopless miniature antenna wire. The short-range receiver profile makes the vicinity of the wire visible.

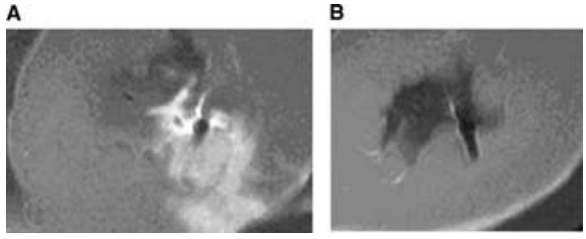

Figure 4. T1 weighted high-resolution short-axis images of the LV for assessment of transmural gadolinium distribution after injection (A) and catheter position. Image (B) shows the needle tip in the myocardium as black artifact (B).

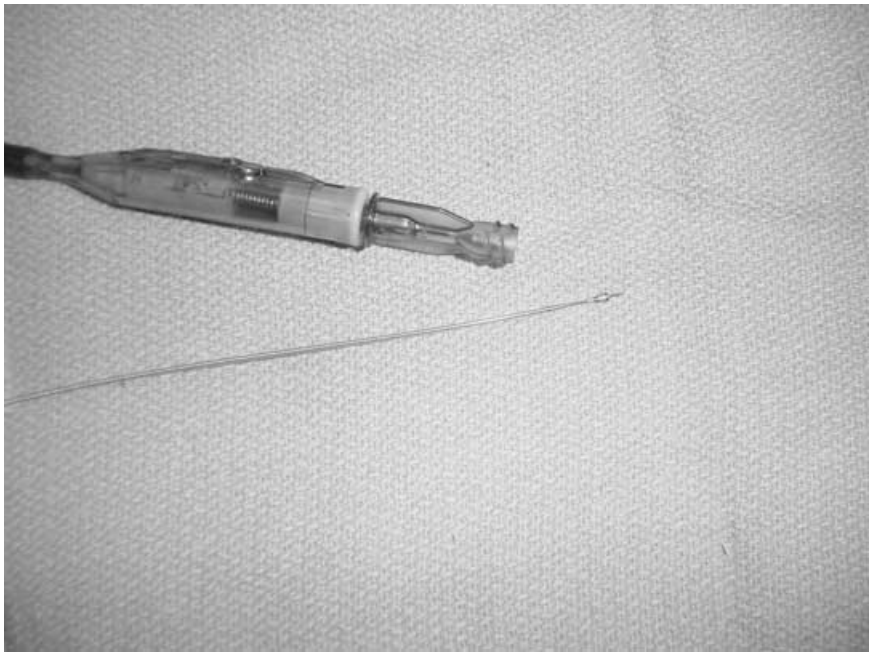

Figure 5. The stem cell catheter is constructed of nitinol without any ferromagnetic parts. This design accounts for its paramagnetic properties resulting in an artifact proportional to the catheter dimensions.

parameters: TR/TE = 2.3/1.8 ms, flip angle 60°; 256 read-out points × 100 phase encodings; 260 mm field of view; band with 900 Hz/pixel).

Cine Imaging and Delayed Enhancement. Gradient echo cine, as well as T1 and T2 weighted spin-echo anatomical imaging was performed, before and after the intervention, to rule out any vascular or cardiac damage, and to assess the extent of gadolinium distribution. Gradient-echo cine images for a short-axis view were obtained to cover the entire cardiac cycle with approximately15 phases (TR per *k*-space segment/TE/flip angle = 1180 ms/4.8 ms/20°). After

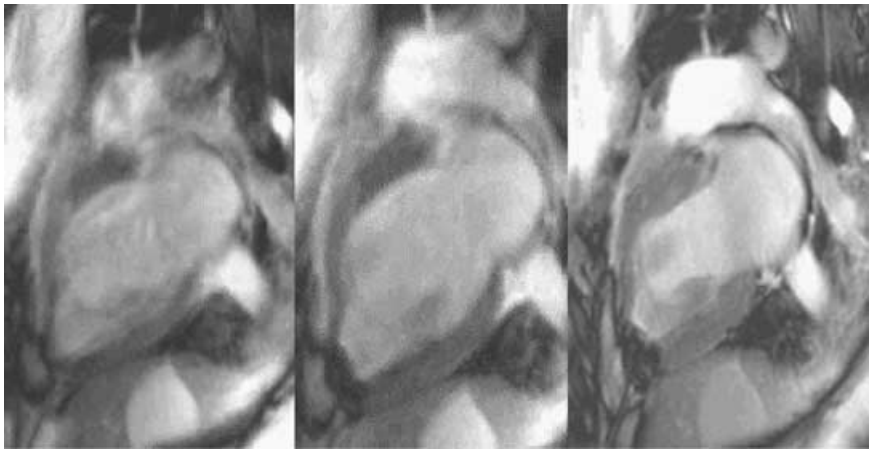

Figure 6. Series of long-axis four-chamber snapshots using a "true FISP" real-time imaging sequence during gadolinium blue dye injection. For real-time imaging the spatial resolution was reduced to increase the temporal resolution up to 8 frames per second. The black artifact results from the high concentrated gadolinium content that was injected leading to signal void.

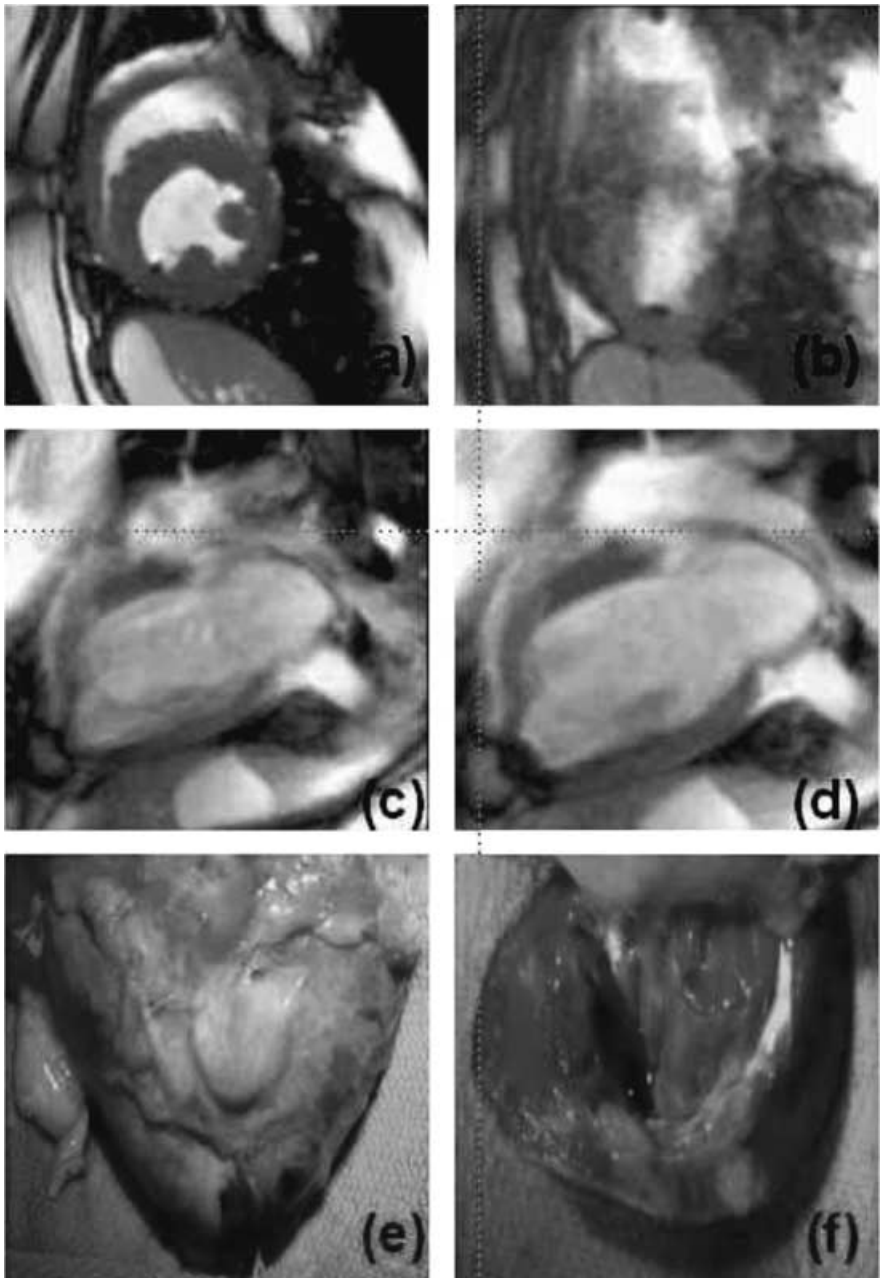

Figure 7. High-resolution T1-weighted short-axis images of catheter position at the pappilary muscle (A) and at the apex (B) under real-time fluroscopy. Long-axis images for pre- (C) and postinjection (D). Postmortem examination of the heart showing the apex (E). The endocardial injected blue dye is also visible on the epicardial surface (F).

completion of the cine and spin-echo imaging, delayed enhancement images were acquired 15–20 minutes after a bolus injection of 0.24 mmol/kg Gd-DTPA with a T1-weighted three-dimensional FLASH sequence with inversion recovery preparation (TR = 420–550 ms, TE = 1.79 ms, TI = 180–220 ms, flip angle 52–65°, FOV = 300 mm, acquisition matrix = 256 × 168, slice thickness 2 mm, total 20–26 slices to encompass the entire LV. These images were later compared to pathology (Fig. 7).

For cine analysis (MASS software, Leiden, Netherlands) endo- and epicardial borders of the LV were defined each in the end-diastolic and end-systolic frame in contiguous slices and standard LV function parameters were calculated to evaluate resting LV function.

Myocardial Perfusion Imaging. Perfusion imaging was performed after the infusion of Gd-DTPA to estimate the myocardial blood flow. The images were acquired with a cardiac-gated, T1-weighted turbo-FLASH sequence with a saturation-recovery magnetization preparation (repetition time: TR = 2.4 ms; echo time: TE = 1.2 ms; delay after saturation pulse: TI = 10 ms; flip angle: $\alpha = 18^{\circ}$; 80–90 phase encoding steps × 128 read-out points with over-sampling; rectangular field of view = 300 mm; receiver bandwidth = 100 kHz; 10 mm slice thickness). Contrast agent dosages of 0.04 mmol/kg of Gd-DTPA (Magnevist, Berlex, Wayne, NJ) were bolus-injected through a venous line at a rate of 7 mL/s. The contrast injection with power injector was performed after starting ECG-gated imaging and coincided approximately with the acquisition of the 5th or 6th image in a series of 50–60 images. Imaging was performed at rest and after the infusion of adenosine (Dosage: 200 μg/mg/min).

Region-of-interest signal intensity curves were generated with the MASS cardiac MRI image analysis software (Laboratory for Clinical and Experimental Image Processing, Leiden University, The Netherlands) by manually segmenting the endocardial and epicardial borders of the images. The segmented myocardium enclosed by the endo- and epicardial borders was then subdivided into eight segments of equal circumferential extent along the myocardial centerline dividing the two contours. The segments were adjusted to start at the anterior junction of the left and right ventricles. Signal intensity–time curves were obtained by averaging the signal intensity in each myocardial segment and for every one of the 50–60 acquired images per slice. The mean value of the signal in each curve prior to the appearance of the contrast agent was subtracted to obtain baseline-corrected signal curves. The baseline-corrected signal curves were further scaled to compensate for spatial inhomogeneities in the sensitivity profile of the receiver radio frequency coil.

The individual tissue signal curves were deconvolved from the intensity curve for the LV obtained from the region encompassed by the endocardial border. A Fermi function model of the myocardial impulse response was used for deconvolution of the myocardial signal intensity curves with an arterial input, measured in the center of the LV. A model trust region algorithm is used for nonlinear estimation of the Fermi parameters.[34] The initial value of the tissue impulse residue represents the mean blood flow in mL/min/g.[34–38]

The ratio of the mean blood flow values for hyperemia and rest was obtained to assess the myocardial perfusion reserve index (MPRI). The values of this index for the target region and a remote region diametrically opposite to that of the target region are compared to assess the perfusion in the infarcted zone.

Myocardial Tissue Tagging. The tagging preparation consisted of nonselective radio frequency pulses separated by encoding gradients for spatial modulation of magnetization, which resulted in a separation of the tag lines of 6 mm. Three to four base-to-apex short-axis cross sections were prescribed to assess regional LV function. At each slice level, two sets of cine images were acquired with tag lines in orthogonal directions. The MR scanning parameters were 300 mm field of view, 256 × 160 acquisition matrix, read-out bandwidth = ±32 kHz, tagging separation of 6 mm, 8 mm slice thickness, TR = 6.5 ms, TE = 2.1 ms, flip angle 15°, and a minimum of 15 cardiac phases. Tagged cine images were only acquired for resting conditions in this study.

Tagged data were analyzed using a custom written analysis package (HARP version 2.0, Nael Oesman, Johns Hopkins Medical School). The technical aspects of HARP have been described in detail elsewhere.[39,40] Two-dimensional myocardial strains were assessed off-line in 12 pie-shaped myocardial segments. Transmural strains were assessed between the reference (end-diastole) and the deformed state (end-systole) as fractional change in length in the circumferential (Ecc) and radial directions (Err) in the subendocardial, midwall, and subepicardial layers. A negative value stands for compression of line segment between two material points (shortening or thinning), while positive values reflect elongation (stretching or thickening), depending on the direction of deformation (circumferential or radial, respectively).

Results

Catheter Tracking and MR-guided Myocardial Injections. MR fluoroscopy with a fast gradient echo sequence with steady-state free precession ("true FISP") could be performed at a sufficiently high frame rate to steer the antenna-guiding catheter in the aorta and the left ventricle. The real-time interactive user

interface allowed interactive specification of the image plane and rapid image reconstruction with a delay of less than 1 s between image acquisition and image display. The spatial in-plane resolution was high enough to see the stem cell delivery catheter (Fig. 3). With interactive control of the slice position, it was possible to continuously verify the anatomical position of the guidewire and/or the sheath with the stem cell delivery catheter in place, a procedure that would have been very cumbersome without interactive slice prescription.

The real-time fluoroscopy technique is currently being further improved to allow interactive road mapping. The injection of the Gd/blue dye could be monitored in all animals. Delayed contrast enhancement imaging with an inversion recovery sequence and high resolution (matrix: 256 × 256; FOV 180), showed the transmural distribution of the gadolinium postendocardial injection. These findings were confirmed by necropsy (Fig. 7).

Myocardial Perfusion. At baseline, the measured myocardial perfusion reserves (MPR) for the target region in the control and treatment groups did not show statistically significant differences. The control group exhibited a moderate decrease of MPR in the ischemic and/or infracted area at the 1-month time point, while there was no significant decrease in the case of the treatment group. Based on the preliminary date of 4 animals (2 treated and 2 control), at the 2-month time point, the treatment group showed a marked improvement with the MPRs (Fig. 8) improving to the levels of normal myocardium, while the MPRS of the control group remained the low.

Myocardial Tissue Tagging. Two-dimensional (2D) myocardial strain assessment was completed for all time points using HARmonic Phase (HARP) image analysis. Mean circumferential shortening in the infarct region reveals significant and sustained long-term improvement in regional function following stem cell therapy in this myocardial ischemia model (Fig. 9). We note that the LV infarct size, measured by delayed contrast enhancement, was not significantly different between groups at baseline (8.56% ± 4.59% exp.; 6.74% ± 2.66% Con.).

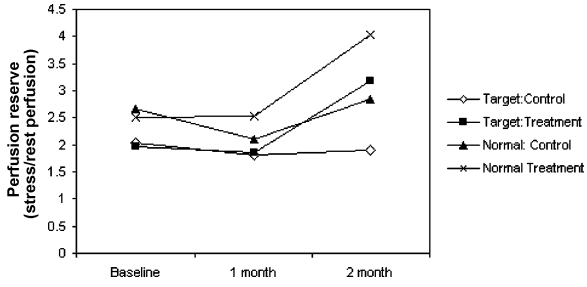

Figure 8. Mean perfusion reserve in chronic domestic large animal infarct model. The preliminary results are reported for regions of remote (noninfarct) and target (ischemic) myocardial segments for two stem-cell-treated and to control animals.

Discussion

The latest generation of interactive cardiac MR scanners capable of applying ultrafast and high-resolution MR imaging techniques have made it possible to perform MR-guided cardiovascular procedures. Real-time imaging with interactive control of the tomographic imaging planes can be used to steer catheters and devices during MRI-guided interventional procedures, as previously demonstrated.[18–21]

In this in vivo study, we demonstrated the feasibility of MR-guided myocardial gadolinium/blue dye injections with a nonferromagnetic stem cell delivery catheter that was used in combination with a newly developed miniature antenna guidewire.[20] In a myocardial infarct model we applied MR perfusion and myocardial strain imaging to investigate the therapeutic effects of myocardial stem cell injections in comparison with sham-treated animals. The preliminary results from this study suggest that myocardial stem cell therapy leads to improvements in both regional function and myocardial perfusion. Myocardial function was only assessed during resting conditions, and this study therefore leaves open the question of whether the improvement of the perfusion reserve is matched by an improvement of the contractile reserve. Myocardial perfusion was measured both at rest and during maximal vasodilation with adenosine. The increase of the myocardial perfusion reserve in the treated animals could be indicative of an improved collateral circulation as a result of stem cell therapy.

Catheter Tracking and Myocardial Stem Cell Injections. Guidewire and catheter tracking are a prerequisite for MRI-guided targeting of myocardial injections. We used a novel loopless miniature antenna guidewire for active tracking in the aorta and the heart.[20] The very high signal intensities from tissue and blood in close vicinity to the antenna resulted in a projection-type image (Fig. 5). The principles of active and passive tracking methods have been described

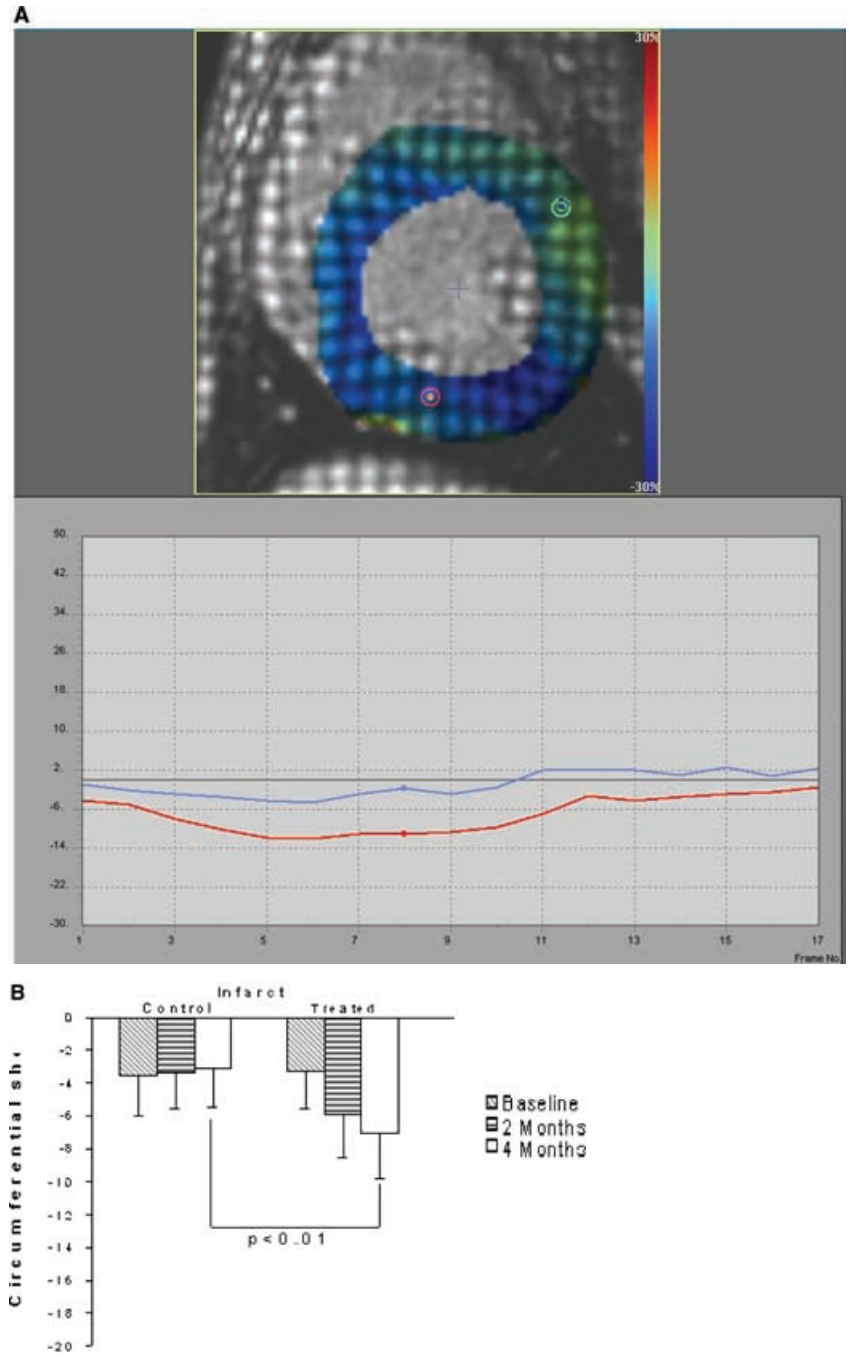

Figure 9. Circumferential shortening (A) in the infarct region for control versus stem-cell-treated animals followed serially by MRI HARP Imaging demonstrates a significant ($P < 0.01$) improvement at 4 months of treatment (B).

in detail elsewhere.[16] Once the delivery sheath was placed in a stable position in the left ventricle, the antenna guidewire was taken out and a newly developed stem cell delivery catheter (Boston Scientific) was pushed into the LV. This catheter with its nitinol composition has paramagnetic properties resulting in susceptibility artifacts ideally suited for passive tracking (Fig. 4).

Before the myocardial injection was performed, high-resolution imaging to identify the position of the catheter was performed (Fig. 3). Following these steps, an injection of gadolinium/trypan blue was performed under real-time MRI (Fig. 6). We were able to continuously verify the anatomical position of the catheter using a real-time imaging frame rate of 5–8 images/s. After the injection, the gadolinium distribution was imaged using T1 and T2 weighted turbo spin-echo sequences (Fig. 7A and B) and an inversion recovery pulse sequence for late enhancement (Fig. 7C and D). These results correlated well with gross pathology findings (Fig. 7E and F).

Effects of Stem Cell Therapy. Within the same MRI set-up used for the MRI-guided intervention we followed the effects of stem cell therapy by quantification of myocardial perfusion measurement (Fig. 8) and tissue tagging (Fig. 9). Both these MRI protocols indicate improvements in the infarcted myocardial tissue as a result of stem cell therapy. By combining images from multiple slice positions in the heart it is possible to generate a three-dimensional model of the heart with surface rendering of the delayed contrast enhancement to visualize the infarcted region (Fig. 10) and to guide the effect of stem cell therapy.

These initial results from animal studies support the rationale for further improvements of MR-guided cardiac stem cell injections, both in terms of developing improved MRI-compatible catheters and catheter antennas, and in terms of optimizing the stem cell therapy protocol. The minimally invasive nature of MRI-guided stem cell injections should facilitate the optimization of stem cell injection protocols, including repeated stem cell injections, an approach that would impose a formidable burden on patients if requiring repeat thoracotomies.

Current experience with myocardial stem cell therapy has not yet established optimal dosages and time-courses for this very promising therapeutic regimen. Cardiac MRI may play a unique role in elucidating the value of stem cell protocols. Furthermore, cardiac MRI allows a multifaceted evaluation of anatomy, function, perfusion, and regional contraction, in the same setting as the MRI-guided stem cell injections, and this may ultimately lead to a better understanding of myocardial pathophysiology, as well as the effects of stem cell therapy. Our results indicate that stem cell therapy in a chronic ischemia model may induce improvement in cardiac function and perfusion, which are the basis of ongoing experimental trials in cardiac stem cell therapy.

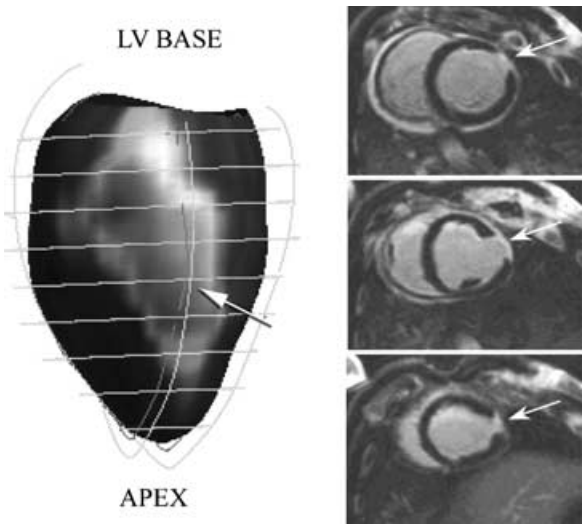

Figure 10. Three-dimensional modeling of myocardial wall motion quantification from late enhanced images showing the infarcted region.

Conclusions

In this in vivo study, we demonstrated the feasibility of MR-guided myocardial gadolinium/blue dye injections using a nonferromagnetic stem cell delivery catheter in conjunction with a newly developed miniature antenna guidewire. These pilot animal studies will serve as templates for future studies with MR-guided cardiac stem cell injections. Furthermore, we demonstrated that cardiac MRI allows a mulitcategorial approach of evaluating anatomy, function, perfusion, and regional contractile parameters in one examination, which may lead to a better understanding of the myocardial pathophysiology as well as the effects of stem cell therapy. These results, not previously reported, suggest that stem cell therapy in a chronic ischemia model may induce improvement in cardiac function and perfusion. In the future, this technique may offer a combined approach of interventional and diagnostic cardiac imaging for stem cell therapy in humans.

Acknowledgments: Dr. Rickers was supported in part by a grant from the German Research Society (DFG no. RI 1040/1-1). Dr. Gallegos was supported by a grant from the Lillehei Heart Institute and by the Richard Varco Surgical Research Fellowship.

References

1. Wang JS, Shum-Tim D, Galipeau J, et al. Marrow stromal cells for cellular cardiomyoplasty: Feasibility and potential clinical advantages. J Thorac Cardiovasc Surg 2000;120(5):999–1005.
2. Orlic D, Kajstura J, Chimenti S, et al. Bone marrow cells regenerate infarcted myocardium Nature 2001;410(6829):701–705.
3. Atalar E, Bottomley PA, Ocali O, et al. High resolution intravascular MRI and MRS by using a catheter receiver coil. Magn Reson Med 1996;36:596–605.
4. Bakker CJ, Hoogeveen RM, Weber J, et al. Visualization of dedicated catheters using fast scanning techniques with potential for MR-guided vascular interventions. Magn Reson Med 1996;36:816–820.
5. Rickers C, Lardo A. High-resolution intravascular and intracardiac MRI. International Symposium on Medical Imaging and Augmented Reality (MIAR), Hong Kong, 2001.
6. Dumoulin CL, Souza SP, Darrow RD. Real-time position monitoring of invasive devices using magnetic resonance. Magn Reson Med 1993;29:411–415.
7. Hu X, Parrish T. Reduction of field of view for dynamic imaging. Magn Reson Med 1996;31:691–694.
8. Kerr AB, Pauly JM, Hu BS, et al. Real-time interactive MRI on a conventional scanner. Magn Reson Med 1997;38:355–367.
9. Keeler EK, Casey FX, Engels H, et al. Accessory equipment considerations with respect to MRI compatibility. J Magn Reson Imaging 1998;8:12–18.
10. Lardo AC, McVeigh ER, Atalar E, et al. Magnetic resonance guided radiofrequency ablation: Visualization and temporal characterization of thermal lesions. Circulation 1998;98:3385.
11. Lardo AC. Real-time MRI: Diagnostic and interventional applications. Pediatr Cardiol 2000;21(1):80–98.
12. Lardo AC. Real-time MRI applications plasty: In vitro demonstration of the potential of MRI for guiding, monitoring, and evaluating endovascular interventions. J Magn Reson Imaging 1999;8:245–250.
13. Ladd ME, Erhart P, Debatin JF, et al. Guidewire antennas for MR fluoroscopy. Magn Reson Med 1997;37:891–897.
14. Lardo AC, McVeigh ER, Jumrussirikul P, et al. Visualization and temporal/spatial characterization of cardiac radiofrequency ablation lesions using magnetic resonance imaging. Circulation 2000;102(6):698–705.
15. McKinnon GC, Debatin JF, Leung DA, et al. Towards active guidewire visualization in interventional magnetic resonance imaging. MAGMA 1996;4:13–18.
16. Rickers C, Seethamraju RT, Jerosch-Herold M, et al. Magnetic resonance imaging guided cardiovascular interventions in congenital heart diseases. J Interven Cardiol 2003;16(2):143–147.
17. Reeder SB, Atalar E, Faranesh AZ, et al. Multi-echo segmented k-space imaging: An optimized hybrid sequence for ultrafast cardiac imaging. Magn Reson Med 1999;41:375–385.
18. Lederman RJ, Guttman MA, Peters DC, et al. Catheter-based endomyocardial injection with real-time magnetic resonance imaging. Circulation 2002;105(11):1282–1284.
19. Bakker CJ, Smits HF, Bos C, et al. MR-guided balloon angioplasty: In vitro demonstration of the potential of MRI for guiding, monitoring, and evaluating endovascular interventions. J Magn Reson Imaging 1998;8(1):245–250.
20. Rickers C, Gallegos R, Bolman C, et al. MRI guided myocardial injections using a novel stemcell delivery catheter. J Cardiovasc Magn Reson 2003;(5):219, Abstract #371.
21. Garot J, Unterseeh T, Teiger E, et al. Magnetic resonance imaging of targeted catheter-based implantation of myogenic precursor cells into infarcted left ventricular myocardium. J Am Coll Cardiol 2003;41(10):1841–1846.
22. Gage FH. Mammalian neural stem cells. Science 2000; 287(5457):1433–1438.
23. Potten CS. Stem cells in gastrointestinal epithelium: Numbers, characteristics and death. Philos Trans R Soc Lond B Biol Sci 1998;353(1370):821–830.
24. Watt FM. Epidermal stem cells: Markers, patterning and the control of stem cell fate. Philos Trans R Soc Lond B Biol Sci 1998;353(1370):831–837.
25. Fridenshtein AI. Stromal bone marrow cells and the hematopoietic microenvironment. Arkh Patol 1982;44(10):3–11.
26. Makino S, et al. Cardiomyocytes can be generated from marrow stromal cells in vitro. J Clin Invest 1999;103(5):697–705.
27. Wakitani S, Saito T, Caplan AI. Myogenic cells derived from rat bone marrow mesenchymal stem cells exposed to 5-azacytidine. Muscle Nerve 1995;18(12):1417–1426.
28. Reyes M, Verfaillie CM. Characterization of multipotent adult progenitor cells, a subpopulation of mesenchymal stem cells. Ann NY Acad Sci 2001;938:231–233 (discussion: pp. 233–235).
29. Martin AI, Piewes DB, Henkelman MR. MR imaging of blood vessels with an intravascular coil. Magn Reson Imaging 1992;2:421–429.
30. Ocali O, Atalar E. Intravascular magnetic resonance imaging using a loopless catheter antenna. Magn Reson Med 1997;37:112–118.
31. Quick HH, Ladd ME, Nanz D, et al. Vascular stens as RF antenna for intravascular MR guidance and imaging. Magn Reson Med 1999;42:738–745.
32. Susil RC, Yeung CJ, Halperin HR, et al. Multifunctional interventional devices for MRI: A combined electrophysiology/MRI catheter. Magn Reson Med 2002;47(3):594–600.
33. Spuentrup E, Ruebben A, Schaeffter T, et al. Magnetic resonance-guided coronary artery stent placement in a swine model. Circulation 2002;105(7):874–879.
34. Jerosch-Herold M, Wilke NM, Stillman AE, et al. MR quantification of the myocardial perfusion reserve with a Fermi model of constrained deconvolution. Med Phys 1998;25:73–84.
35. Jerosch-Herold M, Rickers C, Wilson B, et al. Myocardial blood flow in asymptomatic men and women measured with MRI. Circulation 2002; Vol. 106, No. 9 (Suppl.)3405.
36. Wilke N, Jerosch-Herold M, Stillman AE, et al. Concepts of myocardial perfusion imaging in MRI. Magn Reson Q 1994;10:249–286.
37. Wilke N, Jerosch-Herold M, Wang Y, et al. Multi-slice quantitative first pass imaging assessment of myocardial perfusion reserve. Radiology 1997;204:373–384.
38. Wilke NM, Jerosch-Herold M, Zenovich A, et al. Magnetic resonance first-pass myocardial perfusion imaging: Clinical validation and future applications. J Magn Reson Imaging 1999;10:676–685.
39. Osman NF, McVeigh ER, Prince JL. Imaging heart motion using harmonic phase MRI. IEEE Trans Med Imaging 2000;19(3):186–202.
40. Osman NF, Kerwin WS, McVeigh ER, et al. Cardiac motion tracking using CINE harmonic phase (HARP) magnetic resonance imaging. Magn Reson Med 1999;42(6):1048–1060.